Minimal model of inelastic tunneling of vibrating magnetic molecules on superconducting substrates

Athanasios Koliogiorgos [*]
Department of Condensed Matter Physics, Faculty of Mathematics and Physics, Charles University, 121 16 Prague, Czech Republic

Richard Korytár [†]
Department of Condensed Matter Physics, Faculty of Mathematics and Physics, Charles University, 121 16 Prague, Czech Republic and Institute of Theoretical Physics, University of Regensburg, 93040 Regensburg, Germany

(Received 21 March 2024; revised 6 November 2024; accepted 10 December 2024; published 20 December 2024)

We present an efficient method of calculating the vibrational spectrum of a magnetic molecule adsorbed on a superconductor, directly related to the first derivative of the tunneling IV curve. The work is motivated by a recent scanning-tunneling spectroscopy of lead phthalocyanine on superconducting Pb(100), showing a wealth of vibrational excitations, the number of which highly exceeds molecular vibrations typically encountered on normal metals. We design a minimal model, which represents the inelastic transitions by the spectral function of a frontier orbital of the molecule in isolation. The model allows for an exact solution; otherwise the full correlated superconducting problem would be hard to treat. The model parameters are supplied from an *ab initio* calculation, where the presence of the surface on the deformation of molecular geometry can be taken into account. The spectral function of the highest-occupied molecular orbital of the anionic $PbPc^{1-}$ shows the best agreement with the experimental reference among other molecular charge states and orbitals. The method allows us to include multiple vibrational transitions straightforwardly.

DOI: 10.1103/PhysRevB.110.235424

I. INTRODUCTION

The experimental ability to contact single molecules (through scanning-tunneling, break-junction, and other techniques) made it possible to study molecular many-body excitations by electron transport [1–3]. Unlike in optical spectroscopies, the excitation energy is provided by the tunneling electron, whose energy is controlled by the voltage bias V across the junction. Magnetic molecules play a prominent role here because their low-bias electron transport spectra can be endowed with inelastic spin transitions or Kondo peaks, if the contacts are normal metals. If one or two contacts are superconducting, a narrow in-gap resonance, known as Yu-Shiba-Rusinov peak, may arise [4]. In molecules, these spin-excitations often reflect interactions with other orbital and vibrational degrees of freedom [5–9], thus providing insights into the many-body processes at molecular scale and the way the chemical environment affects them [10–13].

In a recent paper, Homberg *et al.* have reported resonances in a PbPc molecule on a superconducting Pb(100), which they attributed to vibrational excitations [14]. These excitations appeared as peaks in the first derivative of the current-voltage relation, $I(V)$, within the superconducting gap, in a scanning-tunneling setup. The spectra of Ref. [14] are exceptional as they deliver more than 40 sharp peaks in the $\mathrm{d}I/\mathrm{d}V$, compared to the commonly encountered single peak in the normal-state $\mathrm{d}^2I/\mathrm{d}V^2$ of molecular junctions and adsorbates (see Ref. [3] for a review). Undoubtedly, the observation paves way to obtaining valuable information about the adsorbate and its processes from the vibrational spectrum. Nonetheless, the price to pay for such wealth of peaks is that the theoretical description is very challenging. Apart from the complexity of vibrational transitions in presence of an electronic continuum, the system is superconducting and the molecule is paramagnetic due to Coulomb blockade. At present, efficient solution of the problem is not available even for simplified model Hamiltonians that exclude the atomistic details. However, it is possible to gain valuable insights into the vibrational transitions from pragmatic approaches that simplify the problem to a form tractable by an *ab initio* method. This is the attitude taken in Ref. [14]. In this paper we offer an alternative *ab initio* strategy.

The authors of Ref. [14] employed density-functional theory (DFT) calculations of the electronic and vibrational structure of the PbPc/Pb(100). The results were fed into a nonequilibrium Green's function technique to calculate the electric current as a function of voltage, $I(V)$, which includes the electron-phonon coupling in a lowest-order expansion. This technique operates in a normal-state metal, therefore it includes spurious renormalizations of the vibrations (e.g., frequency shifts) from the (ungapped) Fermi surface. Moreover, the first derivative, $\mathrm{d}I/\mathrm{d}V$, produces steplike transitions instead of sharp peaks, because the density of states around the Fermi level is continuous. Despite these conceptual problems, therein reported quantitative agreement with the experiment is fairly good.

In this work we offer an alternative computational approach that avoids the problem of the continuous density of

[*]Contact author: athanasios.koliogiorgos@matfyz.cuni.cz
[†]Contact author: richard.korytar@ur.de

states (spurious metallicity). The central object of our approach is the electronic spectral function of the molecule, which is directly related to the first derivative of the current in the tunneling limit of STM. We calculate the vibrational transitions from given electronic orbitals of the molecule in isolation. The resulting theoretical spectra of PbPc compare well with the experiment and offer an interpretation of correlated electronic transport through the adsorbate.

II. METHODOLOGY

A. Theoretical approach

In scanning-tunneling spectroscopy, the STM tip acts as a probe of the local spectral function of the sample $A(\mathbf{r}, E)$, i.e., the spectrum of electron addition and removal processes at point $\mathbf{r}$ and energy E [15–17]. The latter is directly proportional to the differential conductance,

$$\left.\frac{\mathrm{d}I(V)}{\mathrm{d}V}\right|_{\text{Tip over }\mathbf{r}} = bA(\mathbf{r}, E_\mathrm{F} + V), \tag{1}$$

where E_F is the Fermi energy of the sample and V is the bias voltage. The $A(\mathbf{r}, E)$ is independent on the chemical potential of the tip and the prefactor b is weakly energy dependent. The expression (1) is valid in the tunneling limit of a large tip-sample separation (tip height z); the differential conductance provides information about the sample only, up to a z-dependent prefactor.

If the STM tip is superconducting, the situation is more complicated because of Andreev processes involving the transfer of Cooper pairs. It was shown by Ruby *et al.* [18] that in the large z limit the transport is dominated by single-electron tunneling. The latter is again represented by the $A(\mathbf{r}, E)$, albeit it enters $I(V)$ convoluted by the singular tip density of states. To address electron-vibrational transitions of magnetic adsorbates, we therefore focus on the local spectral function.

The physical basis that allows the observation of rich vibrational spectra in Ref. [14] is the so-called Andreev bound state [19], resulting from interaction of the molecular magnetic moment with the superconducting host, producing sharp peaks in the spectral function inside the superconducting gap. These peaks are often called Yu-Shiba-Rusinov (YSR) resonances. Furthermore, the existence of the magnetic moment of the adsorbed molecule implies Coulomb blockade phenomenon [3]. On top of that, the molecular electronic degrees of freedom interact with vibrations, allowing inelastic transitions in the electron addition (removal) processes. The salient vibrational spectrum results from a combination of complex physical processes: interaction of localized vibrations with delocalized electronic states, superconductivity, and magnetism. At present there are no controlled approximations to this problem; useful insights into the spectra can only be gained from toy models that simplify the problem considerably. We take this pragmatic approach and construct a simplified model that allows part of the problem to be treated *ab initio* to deliver insights taking into account the atomistic details of the electron-vibrational transitions of the molecular tunneling spectra.

The basis of our approach is the assumption that the vibrational spectrum results from vibrational coupling with a discrete (in-gap) electronic resonance, labeled by α. We do not adopt further assumptions regarding the origin of the resonance α. The latter could be viewed as an electron-transporting frontier orbital, as it is common in molecular electronics [3], or the open-shell orbital hosting the Coulomb blockade and YSR resonance. We chose for the α one of the two frontier orbitals and make an unbiased comparison between them.

1. Definition of the minimal model

Given the previously mentioned considerations, we truncate the physical problem to the interaction of a single molecular orbital with molecular vibrations. This familiar many-body problem offers direct access to the electronic spectral function. Given is a single electronic orbital (labeled by α) and discrete independent vibrational excitations $v = 1, \ldots, N_\mathrm{vib}$. The Hamiltonian reads

$$\hat{H} = E_\alpha\, \hat{c}_\alpha^\dagger \hat{c}_\alpha + \sum_v \hbar\omega_v\, \hat{b}_v^\dagger \hat{b}_v + \sum_v \lambda_{\alpha\alpha}^v\, \hat{c}_\alpha^\dagger \hat{c}_\alpha (\hat{b}_v + \hat{b}_v^\dagger), \tag{2}$$

where $\hat{c}_\alpha, \hat{b}_\alpha$ are canonical annihilation operators of the electronic and vibrational degrees of freedom, E_α is the on-site energy of the orbital, ω_v are vibrational frequencies, and $\lambda_{\alpha\alpha}^v$ are (diagonal) electron-vibrational (EV) coupling matrix elements.

In absence of EV coupling ($\lambda_{\alpha\alpha}^v = 0$) the electronic spectral function is $A_\alpha^{(0)}(E) = \delta(E - E_\alpha)$. In presence of finite EV coupling the zero-temperature spectral function is also known exactly [20,21], and reads

$$A_\alpha(E) = A_\alpha^{(0)}(E) + A_\alpha^{(2)}(E) + A_\alpha^{(4)}(E) + \mathcal{O}\big(g_v^6\big) \tag{3a}$$

$$A_\alpha^{(2)}(E) = \sum_v g_v^2\, \delta(E - \hbar\omega_v - E'_\alpha) \tag{3b}$$

$$A_\alpha^{(4)}(E) = \frac{1}{2}\sum_{v,v'} g_v^2 g_{v'}^2\, \delta(E - \hbar\omega_{v'} - \hbar\omega_v - E'_\alpha). \tag{3c}$$

The zero-order term denotes the unperturbed spectral function with E_α substituted by a renormalized E'_α. We will not reproduce the exact formula of the latter as it is of no importance in this work. The remaining terms in (3) describe multiple EV transitions, controlled by the dimensionless coupling constant

$$g_v := \lambda_{\alpha\alpha}^v / \hbar\omega_v. \tag{4}$$

The second-order term $A_\alpha^{(2)}(E)$, decorates the orbital resonance by single vibrational excitations, displaced by the vibrational energy quanta $\hbar\omega_v$ and scaled by the squared coupling constants. The fourth-order term $A_\alpha^{(4)}(E)$ describes electron addition (or removal) accompanied by simultaneous excitations of two vibrations. Therefore it yields a resonance displaced by the sum of two vibrational energies. Higher-order terms are not shown. Finite temperature T subjects the spectral function to corrections of the order of the Boltzmann factor $e^{-\hbar\omega_v/k_\mathrm{B}T}$. The latter number results negligibly small for the experimentally relevant case, $T = 4.2K$ (typical $\hbar\omega = 40$ meV).

In usual inelastic electron tunneling spectroscopy (IETS) of molecules, the EV coupling constants are usually of the order of few percent (see, e.g., the discussion in Ref. [5]), resulting spectral changes are small and two-vibrational excitations are strongly suppressed. In *ab initio* treatments of molecular IETS [22], two-vibrational excitations are discarded based on this reasoning. Here we include two-vibrational processes as shown in the Eq. (3), because some coupling constants reach ≈0.15 (for the case of gas phase neutral PbPc.)

The above defined simplified model allows us to treat a part of the problem by *ab initio*: the molecular vibrational and electronic spectra and their mutual interactions. We employ the Eq. (3) to calculate the spectral function of the PbPc on superconducting Pb(100). We will use *ab initio* DFT to feed the parameters g_v, ω_v. We consider the molecule in isolation (our approach does not work with the electronic continuum of the supporting metal, because it would turn the molecular orbitals into wide resonances). The (renormalized) orbital energy E_α is not determined by the DFT as it results from the YSR physics; it will be treated as an unknown parameter, which globally shifts the zero energy. We choose for α the frontier orbital, either the highest occupied molecular orbital (HOMO) or the lowest unoccupied molecular orbital (LUMO). This approach does not describe the spatial dependence of the spectral function [see Eq. (1)], because the α is an *a priori* unknown parameter. In most cases, electronic transport through single molecules at low bias is dominated by a single frontier orbital. We will comment on this later in Sec. III.

B. *Ab initio* details

1. Geometry selection and relaxation

The PbPc molecule was simulated in real space with DFT, in a finite structure framework, using the program TURBOMOLE, version 7.6 [23–26]. First, a geometry optimization of the molecule was performed. Calculation of the electron-vibration (EV) coupling requires a high degree of accuracy in the DFT parameters. Thus, for the geometry and subsequent calculations, a triple-ζ polarized basis set of the Ahlrichs group was employed, namely def2-TZVP [27]. When needed, the resolution-of-identity approximation was used, along with auxiliary basis sets [28–30]. The calculation was considered converged when the difference in energy between successive self-consistent field (SCF) cycles was smaller than 10^{-8}. Two functionals were used from two levels of theory: the Perdew-Burke-Ernzerhof (PBE) functional of generalized gradient approximation (GGA), and the hybrid functional B3LYP [31–33]. PBE is generally known to predict satisfactorily the structural properties while underestimating the band and HOMO-LUMO gap [34,35]. B3LYP predicts more accurately the electronic structure and is being widely used in molecular simulations, and specifically in the simulation of PbPc molecule [36,37]. Geometry optimization is followed by calculation of the electronic structure, vibrational modes, and, finally, EV coupling.

To approximately account for geometric distortions that PbPc suffers upon adsorption onto Pb(100), we introduce an additional type of PbPc geometry. Namely, we relaxed PbPc in an equilibrium position on top of a nonperiodic Pb(100) slab consisting of 114 atoms. The Pb(100) slab was converged without further relaxing the geometry, with an initial geometry based on bulk Pb(100), so that it approximates more accurately a two-dimensional (2D) surface, as a fully relaxed slab comprising of 114 atoms has a much more distorted geometry compared to a 2D material. The coordinates of the slab remained fixed during the PbPc relaxation. A D3-DFT dispersion correction was used to account for the van der Waals forces between PbPc and Pb(100) [38]. In order to be able to calculate the binding energy of the compound, the D3 correction was also set for the separate components, so that all calculations were on the same level of theory. The slab atoms were discarded for the EV calculation. By allowing the molecule to fully relax on top of the Pb slab, we were able to determine its binding energy and its final exact position on the surface. The PbPc molecule was oriented with the Pb atom of the molecule pointing away from the substrate, according to the predominant configuration in the experimental study of Ref. [14]. In the experiment, the molecules adsorbed on the Pb(100) surface aggregate into four different orientations [39]. In our calculations, the molecule after relaxation sits on the Pb surface in the way that is depicted in Fig. S10 in the Supplemental Material [40]. This orientation is one of the four in the above-mentioned experiment.

In the experiment of Homberg *et al.* the PbPc presumably turns anionic (and magnetic) when adsorbed as a monolayer [14,39]. The additional electron on the molecule occupies the LUMO (e_g) and the magnetic moment develops due to Coulomb blockade. Therefore, we also calculate anionic $PbPc^{1-}$ with two kinds of geometries. First, a geometry of the neutral PbPc relaxed on the surface. We will refer to this structure as the C_{4v} PbPc/surf. The symmetry assignment is justified in Sec. III. Second, the geometry of relaxed $PbPc^{1-}$ in vacuum. The latter undergoes a Jahn-Teller distortion due to the twofold degeneracy of the e_g LUMO. We refer to this structure as C_{2v} $PbPc^{1-}$. We also calculated the doubly charged anion $PbPc^{2-}$.

2. Electron-vibrational (EV) coupling

We employ a method developed by Bürkle *et al.* and implemented in the latest editions of TURBOMOLE [41–45]. The calculation proceeds in two steps: First, from the standard calculation of vibrations we obtain the eigenvectors of the dynamical matrix $\mathcal{C}^v_\chi$, where χ is an index that refers to atom and spatial direction. This is converted to mass-normalized normal modes $\mathcal{A}^v_\chi = \mathcal{C}^v_\chi/\sqrt{M_k}$ for each k atom, where M_k is the normalized mass. We also obtain the vibrational frequencies ω_v of each of the v normal modes of vibration. (For PbPc, the number of vibrational modes is 171.) Second, from the EV coupling calculation we obtain the first-order derivative of the Kohn-Sham operator with respect to the atomic displacements: $H^e_{\mu\nu,\chi} = \langle\mu|\frac{d\hat{H}^e}{d\chi}|\nu\rangle$, where μ, ν are the basis functions. From these data, we calculate the EV coupling constants

$$\lambda^v_{\mu\nu} = \left(\frac{\hbar}{2\omega_v}\right)^{1/2} \sum_\chi \langle\mu|\frac{d\hat{H}^e}{d\chi}|\nu\rangle \mathcal{A}^v_\chi. \tag{5}$$

Following that, we calculate the dimensionless g_v from the Eq. (3).

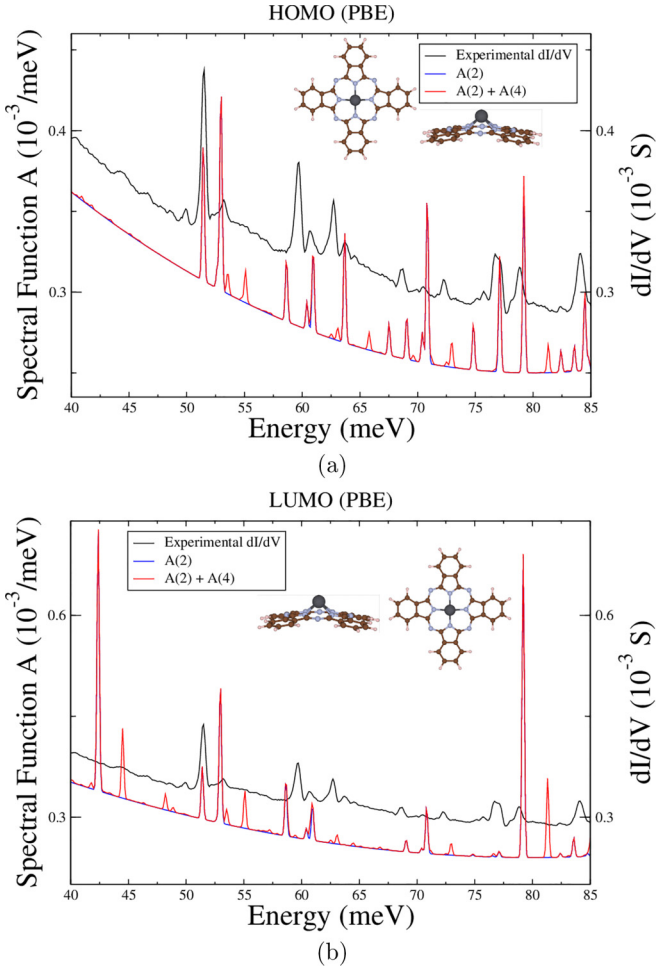

FIG. 1. Spectral function describing single $[A_\alpha^{(2)}(\omega)]$ and double $[A_\alpha^{(4)}(\omega)]$ electron-vibrational transitions from the molecular orbitals (a) $\alpha =$ HOMO and (b) $\alpha =$ LUMO using the PBE functional, for the C_{4v} PbPc relaxed in vacuum (see inset for the model). The experimental dI/dV spectrum from Ref. [14] is included. To facilitate comparison, a polynomial background has been added to the theoretical spectrum.

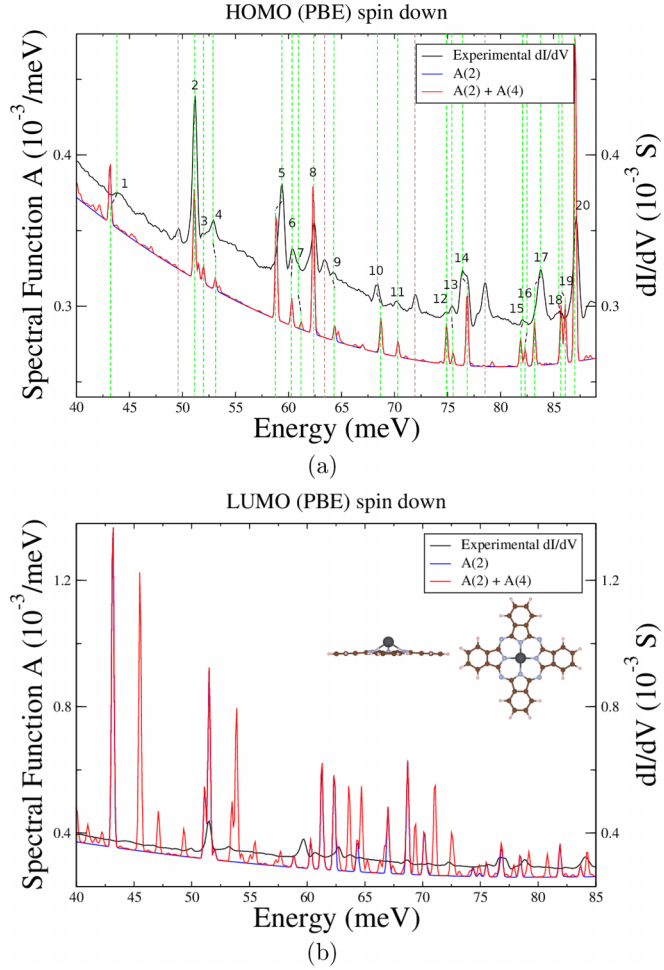

FIG. 2. Spectral function describing single $[A_\alpha^{(2)}(\omega)]$ and double $[A_\alpha^{(4)}(\omega)]$ electron-vibrational transitions from the minority-spin molecular orbitals $\alpha =$ HOMO (a) and LUMO (b) using the PBE functional, of $PbPc^{1-}$ with the C_{4v} PbPc/surf structure. The 20 highest experimental peaks are numbered in (a). Green dotted lines indicate energies for which there is an evident correspondence between experimental and theoretical peaks. Brown dotted lines represent experimental or computational peaks for which there is no correspondence within 1 meV. The green dotted lines, which are connected by a small black dotted line indicate cases where is a small shift in energy. Inset in (b) shows the C_{4v} geometry of PbPc relaxed on top of Pb(100), employed in the calculation.

III. RESULTS

A. Basic properties of PbPc and $PbPc^{1-}$ in isolation and in the potential of Pb(100)

The molecule in isolation relaxes to a nonplanar geometry where the Pb atom is protruded above the Pc plane (see inset of Fig. 1), with a distance of Pb from the Pc plane of 2.15 Å (PBE) and 2.35 Å (B3LYP). The orthogonal distance between the extremes of the Pc plane is 1.23 nm (PBE) and 1.22 nm (B3LYP). The HOMO-LUMO gap is 1.363 eV (PBE) and 2.096 eV (B3LYP). These numbers are in agreement with previous reports [36] and compare well with the experimental data 2.23 Å, 1.23 nm, and 2.01 eV, respectively [46]. We note a near-perfect agreement of the PBE structural parameters with the experiment.

The gas-phase PbPc enjoys a C_{4v} symmetry that results in a doubly degenerate lowest unoccupied molecular orbital (LUMO) (see Supplemental Material, Fig. S5 [40]). Upon charging with one electron, the molecule lowers its total energy by distorting to C_{2v}. As demonstrated in the Supplemental Material, Fig. S9 [40], this is mainly due to folding of one pair of opposite hexagonal lobes, i.e., the B_{1g} mode is the most prominent (cf. also Ref. [47]). The energy of Jahn-Teller distortion is 66.7 meV.

The PbPc molecule in proximity to Pb(100) undergoes a significant structural change as can be seen in the inset of Fig. 2. Instead of the curved structure characteristic of gas phase PbPc, PbPc on Pb(100) turns to almost planar. The molecule after relaxation rests at a distance of approximately 3.5 Å from the Pb(100) surface, in good comparison with the experimental distance of 3.7 Å [14]. The top view of the relaxed adsorption geometry is shown in Supplemental Material, Fig. S10, showing no reduction of molecular

symmetry [40]. We confirm the statement of Homberg *et al.* that stand-alone adsorbate is subject to a negligible charge transfer. The total energy of the PbPc/Pb(100) pair was −23 856.905 Hartree. The energy of the stand-alone PbPc was −1858.744 Hartree, while the energy of the Pb slab was −21 998.08 Hartree. Thus, the binding energy of the PbPc-Pb(100) compound was determined at 0.081 Hartree, or 2.20 eV.

B. Analysis of spectra of PbPc

Figure 1 shows the HOMO and LUMO spectral functions of isolated PbPc alongside with the experimental dI/dV from Ref. [14]. To facilitate comparison, we have blue shifted the experimental spectrum by 1 meV and we have added a second-order polynomial that decreases slowly with energy. The overall prefactor of the theoretical spectrum was adjusted to facilitate the comparison with the experimental data. In the experiment it is largely controlled by the strength of the matrix element representing tunneling from the tip through the vacuum to the molecule. Therefore, only the relative peak heights are sample specific. The theoretical spectrum was convoluted by a Gaussian with broadening 0.1 meV. The dominant contributions to the broadening of the peaks seen in the experiment are the experimental resolution (of the van Hove singularity) and vibrational decay into the phonon continuum. The latter effect should be negligible for vibrational energies higher than the surface band limit. Here, we employ the Gaussian broadening to facilitate the comparison. We also report the unconvoluted data, i.e., the coupling constants g_v [see Eq. (4)] in the Supplemental Material, Fig. S14 [40].

A quick glance through the graphs reveals two energy intervals with distinct performance of the theoretical model. Above ≈30 meV it is possible to match certain theoretical peaks with the experimental ones. Clustering of peaks seen in the experiment is reproduced, although the model peak energies and relative peak heights do not always correspond. We observe that the agreement with the experiment is better for the HOMO than LUMO. For energies below ≈30 meV the model exaggerates peak heights rendering peak identification impossible. This threshold energy is above the phonon band width of lead ≈10 meV [48,49]. The molecular vibrations in this low-energy end are either resonant with the vibrational continuum of the phonon band, or strongly interacting with it, resulting in pronounced energy shifts and damping. A wider spectrum which includes the low-energy range for the case of HOMO is presented in Fig. S11 in the Supplemental Material [40].

Next, we turn to the anionic open-shell $PbPc^{1-}$ with the C_{4v} PbPc/surf structure relaxed on top of the Pb surface, as described in Sec. II. We note that the spin-unrestricted DFT calculation with odd electron count delivers a spin-polarized system.

The spectral functions of minority-spin HOMO and LUMO of $PbPc^{1-}$ with the C_{4v} PbPc/surf geometry are shown in Fig. 2. The agreement with the experiment is again better for the HOMO than it is for LUMO and it is much better than for the molecule in isolation, Fig. 1. The improvement is consistent with the assumption of Homberg *et al.* [14] that PbPc develops a magnetic moment by becoming anionic. The majority-spin spectral function, however, compares much worse, as can be seen in the Supplemental Material, Fig. S2 [40]. We remark that this spin direction is Coulomb blockaded for electron transport in the open-shell Kohn-Sham DFT. The poor agreement in Fig. S2 compared to the minority-spin is therefore consistent with the open-shell state of the molecule.

Finally, we turn to the anion's spectral functions with the C_{2v} $PbPc^{1-}$ geometry, Fig. S12 and Fig. S13 in the Supplemental Material [40]. The comparison with the experimental conductance is much worse in this case. This observation is consistent with the fact that Jahn-Teller distortions tend to be quenched on metallic surfaces, because the electron tunneling rate of the e_g states is much higher than the velocity of the distorting mode.

Summarizing, the spectral function of the minority-spin HOMO of $PbPc^{1-}$ with the C_{4v} geometry shows the best agreement, consistently with the assumptions of Ref. [14]. A closer inspection of Fig. 2(a) shows that out of the 22 most intense experimental peaks, 20 of them have a corresponding theoretical counterpart. The remaining two are not reproduced in the theory curve. For each of the 20 mutually corresponding peaks we extract their energy centers, $E_i^{\rm exp}$ and $E_i^{\rm th}$ and peak heights with relative to the smooth background, $H_i^{\rm exp}$ and $H_i^{\rm th}$, see Supplemental Material, Table I. The average error of the peak energy, 0.286 meV, is very small. We can rationalize the present success by recalling that the vibrational energies are given by total energy differences, which are well represented in DFT. In contrast, the electron-vibrational couplings involve excited-state properties, that are approximated by Kohn-Sham states. Thus, it is perhaps not surprising that the peak heights have much larger error.

In order to quantify the difference (error) between the experimental and various theoretical curves, we introduce the mean deviation (MD) given by

$$\mathrm{MD} = \sqrt{\frac{1}{20}\sum_{i=1}^{20}\left[\left(E_i^{\rm exp}-E_i^{th}\right)^2+\left(H_i^{\rm exp}-H_i^{th}\right)^2W^2\right]}$$

summing the deviations of the peak positions and heights. To account for differing magnitudes, we introduced the weight factor $W = 5000$. The MD for the isolated PbPc is 0.44 and for $PbPc^{1-}$/surf (minority spin) MD = 0.35 (data in Supplemental Material, Table 1 [40]).

Electron-vibrational transitions in molecules obey selection rules imposed by symmetry. The symmetry of the adsorption site ensures that these selection rules translate into the dI/dV of the STM. To see the effect of selection rules, we portray vibrations of the five most intense peaks of C_{4v} $PbPc^{1-}$/surf in Fig. S15. These vibrations reduce the symmetry of the molecule but preserve the mirror plane that is perpendicular to the screen. We recall that due to an unpaired electron, the C_{4v} symmetry of the neutral PbPc is reduced [see Fig. S6(b)] but the mirror plane is preserved.

C. Two-vibrational excitations

The plots of spectral functions not only show $A_\alpha^{(2)}(E)$, but also the inclusion of two-vibration excitations (2VE) in $A_\alpha^{(4)}(E)$. The 2VE peaks are the red peaks, which are not reproduced by the blue trace. Comparison shows that in all

cases the 2VE contribute weakly and the weight of the 2VE peaks tends to decrease with E, consistently with the presence of the frequency in the denominator of (4). We conclude that the 2VE are likely not very important in the measured data of Homberg *et al.*. However, the plots Fig. 1(a) with Fig. 1(b) show sizable 2VE peaks, suggesting that their small weight in the Fig. 2(a) is rather an exception. Hence, the 2VE should be generally expected to pop up in the spectrum in energy range given in similar systems. Note that the inelastic 2VE are routinely disregarded in the standard IETS framework aimed at nonsuperconducting substrates.

D. Further comparisons

Calculations with B3LYP functional were also performed in the two systems as in Fig. S7 and Fig. S8 in the Supplemental Material, but the results were consistently worse than results with PBE [40]. The vibrational modes of the molecule strongly depend on the geometry and, since PBE produced slightly better results with regards to the Pc planar geometry than B3LYP, this could explain the better estimation of EV coupling of PBE.

Next, the interpretation of the experiment involves certain ambiguity regarding the charge of the molecule in question. Namely, an adsorbed stand-alone PbPc on Pb(100) has negligible charge transfer, but the PbPc presumably turns anionic (and magnetic) when adsorbed as a monolayer [14] (a deeper discussion is in the thesis [39]). Therefore, the charge state of molecules within a monolayer will likely be spatially dependent. To complement the calculations of zero- and one-charge states, we have also investigated the HOMO and HOMO-1 spectra of $PbPc^{2-}$. Note that the latter is a closed shell and the two orbitals adiabatically connect with the LUMO and HOMO, respectively, of $PbPc^{0}$. The comparison with measured curve is significantly worse; we direct the reader to the Supplemental Material, Fig. S3 [40]. Hence, the $PbPc^{1-}$ spectral function is the most consistent with the measurement, favoring the scenario of Homberg *et al.* given above.

IV. DISCUSSION

To make a final observation, we adopt a natural assumption that the HOMO orbital of the isolated molecule (hereafter referred to as $HOMO^{0}$) undergoes only small changes as we deform the geometry by mimicking the presence of the surface or add electrons. Specifically, $HOMO^{0}$ is connected to the minority-spin HOMO of $PbPc^{1-}$ and HOMO-1 of $PbPc^{2-}$, as it follows from a Pauli principle. In a similar fashion, the LUMO of the neutral specimen connects to the LUMO of the minority spin $PbPc^{1-}$ and the HOMO of $PbPc^{2-}$. Moreover, it is connected to the HOMO of the majority spin $PbPc^{1-}$, i.e., the magnetic-moment carrying singly occupied molecular orbital. This statement is validated by comparing the spin density of $PbPc^{1-}$ with the molecular orbital isosurfaces of neutral PbPc, shown in Supplemental Material, Figs. S4–S6. The nodal structure of the two orbitals is the same. We will denote the orbitals connected to the LUMO of the neutral PbPc by $LUMO^{0}$. From inspection of Figs. 1, 2, and S1 we conclude that the spectral function of $HOMO^{0}$ is generally giving better agreement with the experiment than the $LUMO^{0}$.

An important feature of our method is the restriction to a single transporting molecular orbital. It is known that if electronic transport is studied at low bias voltage V, it is valid to use a single frontier orbital as long as the other orbitals are energetically well separated [3]. Specifically, it must hold that $\Gamma_i/|E_i - E_F| \ll 1$, where $E_i - E_F$ is the energy of the orbital i from the Fermi level and Γ_i is its level broadening. It appears that this condition is fulfilled for PbPc/Pb(100): in our calculations the level spacing between HOMO-1, HOMO, LUMO and LUMO + 1 of $PbPc^{0}$ is of the order of 1 eV, while $\Gamma \approx 30$ meV [14] (see also the density of states in the Supplemental Material of the latter reference).

The off-diagonal part of the EV coupling $\lambda^{v}_{\mu\nu}$ allows, in principle, transitions between orbitals. Such transitions are weighted additionally by a factor $\approx \Gamma_i/|E_i + \hbar\omega_v - E_F|$ [50,51]. Consequently, the off-diagonal EV terms can be neglected as long as one stays in the single transport-orbital regime. Our method allows us to include more molecular orbitals, as well as transitions involving off-diagonal EV terms. For the specific case of PbPc/Pb(100), a two-orbital calculation would involve external parameters reflecting differences in level alignment and coupling strengths of these orbitals to the substrate.

We observe that the good agreement of our $HOMO^{0}$ results seems to be at odds with the statement in Homberg *et al.* that $LUMO^{0}$ is the main transport channel. We speculate that the reason could be that the disordered character of the PbPc monolayer of Ref. [14] can affect the level alignment in a way that is not accounted for by the periodic calculation. Other reasons can be methodological (dI/dV vs d^2I/dV^2) or possibly multiorbital.

It is known that the YSR resonance appears twice inside the gap: for positive and negative voltages, and these resonances have different heights reflecting differences in electron and hole tunneling. These differences are highly tip dependent and can be seen as spectroscopically non-universal within the context of STM (see the overview in the Sec. III B of Ref. [52]). The asymmetry of the YSR partners applies also to the vibrational side-peaks. In principle, our techniques can be extended to include such effects following the work of Ruby *et al.* [18].

V. CONCLUSIONS

We have developed a minimal exactly solvable model of inelastic tunneling spectrum of vibrating magnetic molecules adsorbed on superconductors. The purpose of the model is to facilitate direct comparisons with experimental data by having its Hamiltonian parameters supplied from an *ab initio* calculation. Although the interaction with Bogoliubov-de Gennes quasiparticles is not included, the advantage of the model is that it formally delivers vibrational peaks in the spectral function, which corresponds to the first derivative of the IV curve, the tunneling conductance. This is in contrast to the output of common *ab initio* inelastic scanning tunneling spectra, which deliver second derivative of the IV curve. Moreover, multiple vibrational transitions are included at almost zero cost.

We apply the method to lead phthalocyanine on superconducting Pb(100) and compare to the recently published

experimental data. We obtain the best agreement for a negatively charged $PbPc^{1-}$, consistent with the conjecture of adsorbed PbPc gaining magnetic moment by ionizing. A detailed comparison of spectra from different molecular orbitals convincingly points out the dominant role of the HOMO in the electron-vibrational transitions. Since the magnetic moment resides on the LUMO, our results reveal the distinct roles of the two orbitals in the correlated low-energy behavior, guiding the design of more elaborate many-body treatments.

ACKNOWLEDGMENTS

We thank R. Berndt for drawing our attention to the experimental results and providing the measured data for comparison. Discussions with M. Bürkle, A. Donarini, and C. S. Garoufalis are acknowledged. We acknowledge support by the Ministry of Education, Youth and Sports of the Czech Republic through the project e-INFRA CZ (ID:90254) and through the project "e-Infrastruktura CZ" (e-INFRA CZ LM2018140) and the Czech Science foundation (Project No. 22-22419S).

[1] G. D. Scott and D. Natelson, Kondo resonances in molecular devices, ACS Nano **4**, 3560 (2010).

[2] E. Scheer and J. C. Cuevas, *Molecular Electronics: An Introduction to Theory and Experiment*, 2nd ed. (World Scientific, Singapore, 2017).

[3] F. Evers, R. Korytár, S. Tewari, and J. M. van Ruitenbeek, Advances and challenges in single-molecule electron transport, Rev. Mod. Phys. **92**, 035001 (2020).

[4] B. W. Heinrich, J. I. Pascual, and K. J. Franke, Single magnetic adsorbates on s-wave superconductors, Prog. Surf. Sci. **93**, 1 (2018).

[5] J.-P. Gauyacq, N. Lorente, and F. D. Novaes, Excitation of local magnetic moments by tunneling electrons, Prog. Surf. Sci. **87**, 63 (2012).

[6] D. Rakhmilevitch, R. Korytár, A. Bagrets, F. Evers, and O. Tal, Electron-vibration interaction in the presence of a switchable Kondo resonance realized in a molecular junction, Phys. Rev. Lett. **113**, 236603 (2014).

[7] E. Minamitani, N. Tsukahara, D. Matsunaka, Y. Kim, N. Takagi, and M. Kawai, Symmetry-driven novel Kondo effect in a molecule, Phys. Rev. Lett. **109**, 086602 (2012).

[8] M. Ruby, Y. Peng, F. von Oppen, B. W. Heinrich, and K. J. Franke, Orbital picture of Yu-Shiba-Rusinov multiplets, Phys. Rev. Lett. **117**, 186801 (2016).

[9] P. Zalom, J. De Bruijckere, R. Gaudenzi, H. S. van ver Zant, T. Novotný, and R. Korytár, Magnetically tuned Kondo effect in a molecular double quantum dot: Role of the anisotropic exchange, J. Phys. Chem. C **123**, 11917 (2019).

[10] D.-J. Choi, P. Abufager, L. Limot, and N. Lorente, From tunneling to contact in a magnetic atom: The non-equilibrium Kondo effect, J. Chem. Phys. **146**, 092309 (2017).

[11] M. Žonda, O. Stetsovych, R. Korytár, M. Ternes, R. Temirov, A. Raccanelli, F. S. Tautz, P. Jelínek, T. Novotný, and M. Švec, Resolving ambiguity of the Kondo temperature determination in mechanically tunable single-molecule Kondo systems, J. Phys. Chem. C **12**, 6320 (2021).

[12] J. Li, S. Sanz, J. Castro-Esteban, M. Vilas-Varela, N. Friedrich, T. Frederiksen, D. Peña, and J. I. Pascual, Uncovering the triplet ground state of triangular graphene nanoflakes engineered with atomic precision on a metal surface, Phys. Rev. Lett. **124**, 177201 (2020).

[13] S. Trivini, J. Ortuzar, K. Vaxevani, J. Li, F. S. Bergeret, M. A. Cazalilla, and J. I. Pascual, Cooper pair excitation mediated by a molecular quantum spin on a superconducting proximitized gold film, Phys. Rev. Lett. **130**, 136004 (2023).

[14] J. Homberg, A. Weismann, T. Markussen, and R. Berndt, Resonance-enhanced vibrational spectroscopy of molecules on a superconductor, Phys. Rev. Lett. **129**, 116801 (2022).

[15] J. Tersoff and D. R. Hamann, Theory of the scanning tunneling microscope, Phys. Rev. B **31**, 805 (1985).

[16] Y. Meir and N. S. Wingreen, Landauer formula for the current through an interacting electron region, Phys. Rev. Lett. **68**, 2512 (1992).

[17] P. Coleman, *Introduction to Many-Body Physics* (Cambridge University Press, Cambridge, 2015), Chap. 9.7.2.

[18] M. Ruby, F. Pientka, Y. Peng, F. von Oppen, B. W. Heinrich, and K. J. Franke, Tunneling processes into localized subgap states in superconductors, Phys. Rev. Lett. **115**, 087001 (2015).

[19] A. V. Balatsky, I. Vekhter, and J.-X. Zhu, Impurity-induced states in conventional and unconventional superconductors, Rev. Mod. Phys. **78**, 373 (2006).

[20] G. D. Mahan, *Many-Particle Physics* (Springer, Berlin, 2000).

[21] A. Nitzan, *Chemical Dynamics in Condensed Phases* (Oxford Graduate Texts, Oxford, 2006), Chap. 12.5.3, p. 444.

[22] T. Frederiksen, M. Paulsson, M. Brandbyge, and A.-P. Jauho, Inelastic transport theory from first principles: Methodology and application to nanoscale devices, Phys. Rev. B **75**, 205413 (2007).

[23] S. G. Balasubramani, G. P. Chen, S. Coriani, M. Diedenhofen, M. S. Frank, Y. J. Franzke, F. Furche, R. Grotjahn, M. E. Harding, C. Hättig *et al.*, TURBOMOLE: Modular program suite for ab initio quantum-chemical and condensed-matter simulations, J. Chem. Phys. **152**, 184107 (2020).

[24] R. Ahlrichs, M. Bär, M. Häser, H. Horn, and C. Kölmel, Electronic structure calculations on workstation computers: The program system turbomole, Chem. Phys. Lett. **162**, 165 (1989).

[25] O. Treutler and R. Ahlrichs, Efficient molecular numerical integration schemes, J. Chem. Phys. **102**, 346 (1995).

[26] M. Von Arnim and R. Ahlrichs, Performance of parallel TURBOMOLE for density functional calculations, J. Comput. Chem. **19**, 1746 (1998).

[27] F. Weigend and R. Ahlrichs, Balanced basis sets of split valence, triple zeta valence and quadruple zeta valence quality for H to Rn: Design and assessment of accuracy, Phys. Chem. Chem. Phys. **7**, 3297 (2005).

[28] K. Eichkorn, O. Treutler, H. Öhm, M. Häser, and R. Ahlrichs, Auxiliary basis sets to approximate Coulomb potentials, Chem. Phys. Lett. **242**, 652 (1995).

[29] K. Eichkorn, F. Weigend, O. Treutler, and R. Ahlrichs, Auxiliary basis sets for main row atoms and transition metals and

their use to approximate Coulomb potentials, Theor. Chem. Acta **97**, 119 (1997).
[30] F. Weigend, Accurate Coulomb-fitting basis sets for H to Rn, Phys. Chem. Chem. Phys. **8**, 1057 (2006).
[31] J. P. Perdew, K. Burke, and M. Ernzerhof, Generalized gradient approximation made simple, Phys. Rev. Lett. **77**, 3865 (1996).
[32] A. D. Becke, Density-functional thermochemistry. III. The role of exact exchange, J. Chem. Phys. **98**, 5648 (1993).
[33] C. Lee, W. Yang, and R. G. Parr, Development of the Colle-Salvetti correlation-energy formula into a functional of the electron density, Phys. Rev. B **37**, 785 (1988).
[34] A. Koliogiorgos, S. Baskoutas, and I. Galanakis, Electronic and gap properties of lead-free perfect and mixed hybrid halide perovskites: An *ab-initio* study, Comput. Mater. Sci. **138**, 92 (2017).
[35] A. Koliogiorgos, C. S. Garoufalis, S. Baskoutas, and I. Galanakis, Electronic and optical properties of ultrasmall ABX_3 (A = Cs, CH_3NH_3/B = Ge, Pb, Sn, Ca, Sr/X = Cl, Br, I) perovskite quantum dots, ACS Omega **3**, 18917 (2018).
[36] Y. Zhang, X. Zhang, Z. Liu, Y. Bian, and J. Jiang, Structures and properties of 1,8,15,22-tetrasubstituted phthalocyaninato-lead complexes: The substitutional effect study based on density functional theory calculations, J. Phys. Chem. A **109**, 6363 (2005).
[37] M. Sumimoto, T. Honda, Y. Kawashima, K. Hori, and H. Fujimoto, Theoretical and experimental investigation on the electronic properties of the shuttlecock shaped and the double-decker structured metal phthalocyanines, MPc and $M(Pc)_2$ (M = Sn and Pb), Dalton Trans. **41**, 7141 (2012).
[38] S. Grimme, J. Antoni, S. Ehrlich, and H. Krieg, A consistent and accurate ab initio parametrization of density functional dispersion correction (DFT-D) for the 94 elements H-Pu, J. Chem. Phys. **132**, 154104 (2010).
[39] J. B. Homberg, Ph.D. thesis, Christian-Albrechts-Universität zu Kiel, Mathematisch-Naturwissenschaftliche Fakultät, 2022.
[40] See Supplemental Material at http://link.aps.org/supplemental/10.1103/PhysRevB.110.235424 for a display of the HOMO and LUMO isosurface plots of the PbPc and $PbPc^{1-}$/surf; spin density plots of $PbPc^{1-}$; Jahn-Teller distortion of $PbPc^{1-}$; top view of PbPc relaxed on a Pb(100) surface; the spectral function of PbPc with the PbPc/surf geometry; of $PbPc^{1-}$ with PbPc/surf geometry (majority spin); of $PbPc^{2-}$; of PbPc with B3LYP functional; of PbPc with the PbPc/surf geometry with B3LYP functional; of PbPc for a larger energy range; plot of EV coupling constants; spectral function of HOMO of $PbPc^{1-}$/surf together with respective vibrational modes; a table with the data for 20 peaks for HOMO of $PbPc^{1-}$/surf.
[41] M. Bürkle, J. K. Viljas, T. J. Hellmuth, E. Scheer, F. Weigend, G. Schön, and F. Pauly, Influence of vibrations on electron transport through nanoscale contacts, Phys. Stat. Sol. b **250**, 2468 (2013).
[42] P. Deglmann, F. Furche, and R. Ahlrichs, An efficient implementation of second analytical derivatives for density functional methods, Chem. Phys. Lett. **362**, 511 (2002).
[43] P. Deglmann and F. Furche, Efficient characterization of stationary points on potential energy surfaces, J. Chem. Phys. **117**, 9535 (2002).
[44] P. Deglmann, K. May, F. Furche, and R. Ahlrichs, Nuclear second analytical derivative calculations using auxiliary basis set expansions, Chem. Phys. Lett. **384**, 103 (2004).
[45] K. Reiter, M. Kühn, and F. Weigend, Vibrational circular dichroism spectra for large molecules and molecules with heavy elements, J. Chem. Phys. **146**, 054102 (2017).
[46] M. Kato, H. Yoshizawa, M. Nakaya, Y. Kitagawa, K. Okamoto, T. Yamada, M. Yoshino, and O. Jun, Unraveling the reasons behind lead phthalocyanine acting as a good absorber for near-infrared sensitive devices, Sci. Rep. **12**, 8810 (2022).
[47] J. Tóbik and E. Tosatti, Jahn–Teller effect in the magnesium phthalocyanine anion, J. Mol. Struct. **838**, 112 (2007).
[48] I. Y. Sklyadneva, R. Heid, K.-P. Bohnen, P. M. Echenique, and E. V. Chulkov, Surface phonons on Pb(111), J. Phys.: Condens. Matter **24**, 104004 (2012).
[49] M. J. Verstraete, M. Torrent, F. Jollet, G. Zérah, and X. Gonze, Density functional perturbation theory with spin-orbit coupling: Phonon band structure of lead, Phys. Rev. B **78**, 045119 (2008).
[50] N. Lorente and M. Persson, Theory of single molecule vibrational spectroscopy and microscopy, Phys. Rev. Lett. **85**, 2997 (2000).
[51] M. Paulsson, T. Frederiksen, and M. Brandbyge, Modeling inelastic phonon scattering in atomic- and molecular-wire junctions, Phys. Rev. B **72**, 201101(R) (2005).
[52] F. von Oppen and K. J. Franke, Yu-Shiba-Rusinov states in real metals, Phys. Rev. B **103**, 205424 (2021).